A Superharmonic Injection based G-band Quadrature VCO in CMOS

Xuan Ding[1], Hai Yu[1], Bo Yu[2], Zhiwei Xu[3], and Q. Jane Gu[1]
[1]High Speed Integrated Circuits and Systems Laboratory, University of California, Davis, USA
[2]Skyworks Solutions, Inc.
[3]Zhejiang University, China
xxding@ucdavis.edu and jgu@ucdavis.edu

***Abstract*— This paper presents a G-band quadrature voltage-controlled oscillator (QVCO) enabled by a superharmonic injection technique. This technique ensures differential phases at the common mode tail current source nodes of two differential oscillators, which are then enforced to generate quadrature outputs. It achieves a maximum output power of -1.54 dBm with the efficiency of 3.2% and the tuning range (TR) from 149.3 GHz to 152.4 GHz. The measured phase noise (PN) is -91.9 dBc/Hz at 1 MHz offset. The IQ outputs are down-converted by an on-chip mixer for phase and amplitude accuracy measurement. The measured I/Q phase mismatch is less than 1.5◦ and amplitude mismatch of less than 0.33 dB over the operating frequency range. The QVCO is implemented in a 28 nm CMOS process, occupying 0.028 mm² chip area.**

***Keywords*—Quadrature voltage-controlled oscillator (QVCO), Self-injection locking, G-band.**

I. Introduction

Mm-waves and sub-THz bands have been attracting increasing interests over the decade in a variety of applications, such as wideband communications, sensing and imaging. To boost communication data rates or extract signal phases, quadrature local oscillator is an essential component to enable high order modulation schemes and signal phase processing [1]. Quadrature signal generation in the mm-wave and sub-THz frequency range is challenging through conventional techniques due to the introduced extra parasitic capacitance by the coupling devices. The method of using a tripler to generate 120 GHz quadrature LOs from 40 GHz quadrature inputs is a traditional way [2]. However, it introduces power-consuming components such as triplers and buffers. Another approach is to couple two oscillators using active or passive networks for quadrature generation. However, this structure has its own challenges. The passive coupling networks employ a phase shifter along the coupling path, and the phase accuracy is hard to guarantee due to its highly frequency dependent resonant networks [3][4]. Active coupling by utilizing transistors adds more power consumption and noise and faces design trade-off between phase accuracy and phase noise (PN) performance in a quadrature oscillator [5]. Superharmonic coupling oscillation is an attractive technique [6][7]. It uses antiphase signals to lock the second harmonics of the two oscillators and enforcing fundamental frequency signals in quadrature phase relation without hurting PN, phase accuracy and TR. However, it is challenging to directly apply this idea to the frequency beyond one hundred GHz due to the difficulties of the generation and injection of 2nd order harmonics.

This paper proposes a full-integrated superharmonic inject-ion based G-band QVCO. The standalone QVCO and I/Q signal test chips were fabricated in a 28 nm CMOS process. Although the intrinsic device f_t is close to 300 GHz, the effective f_t and f_{max} are degraded significantly due to the parasitic effect, leading to lowering oscillation frequency and DC-to-RF efficiency. This work presents techniques in circuit structure, design ideas and layout strategies to overcome these challenges to guarantee the quadrature generation and boost the output power and efficiency. The QVCO efficiently generates accurate I/Q signals from 149.3 to 152.4 GHz.

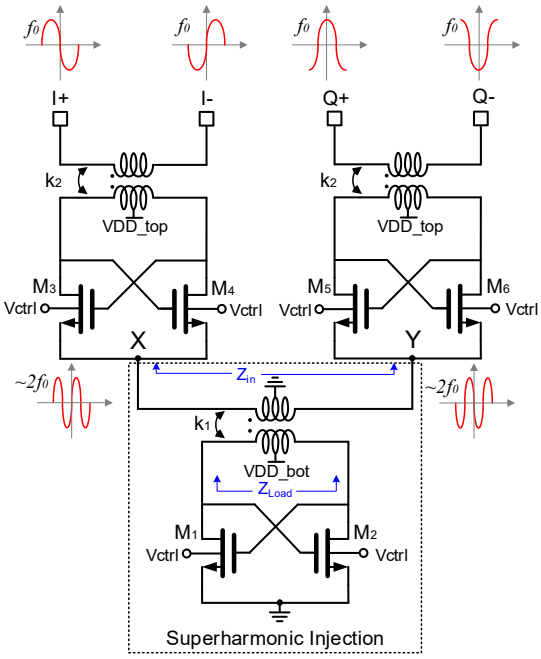

Fig. 1. Schematic of the proposed superharmonic injection based QVCO.

II. QVCO Structure

The QVCO structure is illustrated in Fig.1. The top two oscillators generate differential outputs at fundamental frequency f_0. Their common-mode tail current source nodes are coupled through the bottom oscillator that resonates at frequency $2f_0$. The two tail current source nodes will present anti-phase signals at $2f_0$ if they are successfully injection locked by the bottom one. Because the injection signal is 2nd harmonic of the top oscillation signal, the technique is named superharmonic injection.

The critical factor for quadrature signal generation of this proposed structure is the successful superharmonic injection

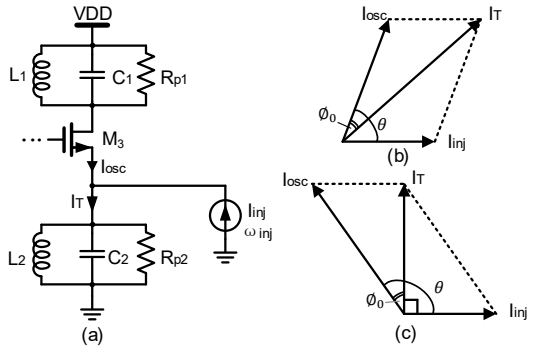

Fig. 2. (a) The equivalent model, (b) phasor relationship, and (c) the maximum phase difference at the edge of injection lock.

operation by the bottom oscillator at $2f_0$. To achieve that, the injection power needs to be strong enough and lock range needs to be sufficiently wide to cover the operating frequency.

Fig. 2 (a) depicts the equivalent injection-lock analysis model. When an injection signal (I_{inj}, ω_{inj}) is added, it is required to satisfy the phasor relationship with I_{osc} and I_T, as shown in Fig. 2 (b) [8]. The angle $\emptyset_0$ between I_{osc} and resultant current I_T, and θ between I_{osc} and I_{inj} satisfy:

$$sin\emptyset_0 = \frac{I_{inj}}{I_T} sin\theta = \frac{I_{inj} sin\theta}{\sqrt{I_{inj}^2 + I_{osc}^2 + 2I_{inj}I_{osc}cos\theta}} \quad (1)$$

At the edge of the lock condition, as shown in Fig. 2 (c).

$$tan\emptyset_0 \approx \frac{2Q}{\omega_0}\left(\omega_r - \omega_{inj}\right) = \frac{I_{inj}}{I_T} \quad (3)$$

Where Q is the tank quality factor and ω_r is the resonant frequency of LC tank. Therefore, the lock range $\pm\omega_L$ is determined as:

$$\omega_L = \omega_0 - \omega_{inj} = \frac{I_{inj}}{I_T}\frac{\omega_0}{2Q} \quad (4)$$

when $I_{inj} \ll I_{osc}$.

$$\omega_L \approx \frac{I_{inj}}{I_{osc}}\frac{\omega_r}{2Q} \quad (5)$$

Lock range is inversely proportional to the quality factor Q, but lowering Q degrades the oscillation output power and efficiency, which is not a good tradeoff in mm-wave/sub-THz design. As a result, boost the injection signal strength is the natural way to increase the lock range.

However, there are challenges even to start the oscillation at such high frequency, not even mention at the 2nd harmonic. First, the device transconductance g_m is extremely low at the frequency close to f_t. Second, the impedance looking into the common mode tail current nodes are relatively low, which drops the equivalent parallel resistance loading to the bottom oscillator to challenge the oscillation condition. To overcome the challenges, a transformer (k1) is inserted between the top and bottom oscillators. First, it supports independent supply and bias of each oscillator to maximize the headroom and transistors' g_m so that it can satisfy the oscillation condition. Second, by adjusting the transformer parameters, including turn ratios and self-inductance etc., the optimum loading can be achieved to the bottom oscillator to increase the signal power and efficiency.

The top transformers (k2) is designed to match to the optimum impedance faced by the core cross-coupled transistor

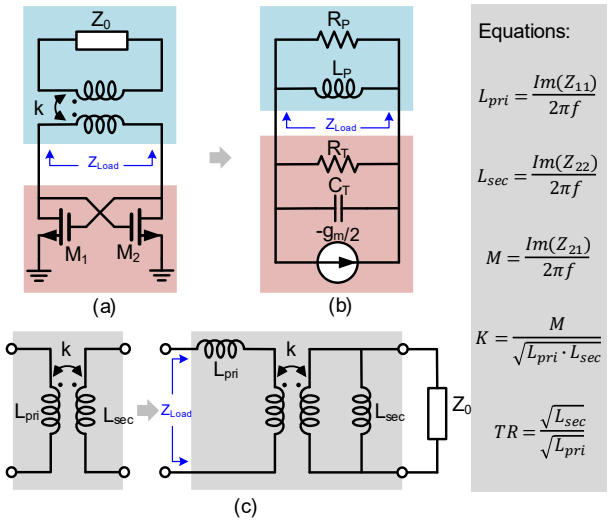

Fig. 3. (a) Schematic of a cross-coupled oscillator, (b) its equivalent circuit, and (c) a transformer and its equivalent lumped model loaded with Zo.

pair. At high frequencies, transformer on the top metal is the best option due to its relatively high Q, which determines the oscillator signal power and efficiency. Besides, transformer-based impedance matching networks provide flexible structures for required impedance conversion ratio, differential interface suitable for cross-coupled transistor pair, and virtual ground in the centre readily for ground or DC power connection.

III. Circuit Design

A. Transformer based cross-coupled oscillator

Fig. 3 (a) depicts a cross-coupled oscillator and its equivalent circuit model, in which R_T is internal equivalent resistance, C_T is total node capacitance, R_P and L_P construct the load Z_L. According to the maximum power transfer theorem, when $R_P = R_T$, the maximum output power is delivered to the load. The other criteria that an oscillator must satisfy is oscillation condition, which is

$$-\frac{g_m}{2} + \frac{1}{R_T} + \frac{1}{R_P} < 0 \quad (6)$$

Therefore,

$$R_P > \frac{1}{\frac{g_m}{2} - \frac{1}{R_T}} \quad (7)$$

In the real case where the circuit is terminated with Z_0, a transformer is employed to realize the impedance matching. Fig. 2(c) shows a transformer model with a series primary coil and a parallel second coil for analysis. Based on the parameters and definitions of the transformer, the input impedance can be calculated.

$$Z_{load} = \frac{K^2}{TR^2} Re(Z_0 // sL_{sec}) + j\left[\frac{K^2}{T^2} Im(Z_0 // sL_{sec}) + \omega L_{pri}\right] \quad (8)$$

Where L_{pri} is the inductance of primary coil; L_{sec} is the inductance of secondary coil; M is the mutual inductance; K is the coupling coefficient; T is turn ratio of the transformer and Z_{load} is the input impedance looking into the primary coil. The equivalent resistance, R_p, parallel with the cross-coupled transistors at the resonant frequency ω_r is obtained as:

$$R_p = \frac{(\omega_r L)^2}{Re(Z_{in})} \quad (9)$$

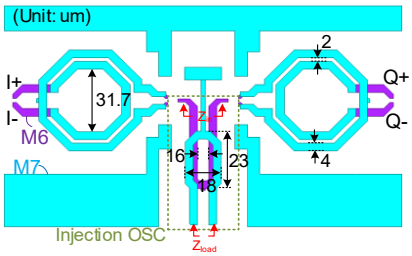

Fig. 4. Top view of the transformer model in EM simulation.

VDD_top (V)	Zin/Z0 @300GHz	Equivalent R & C
1.0	2.17 – j1.45	157 Ω, 2.1 fF
0.8	2.01 – j1.73	175 Ω, 2.4 fF

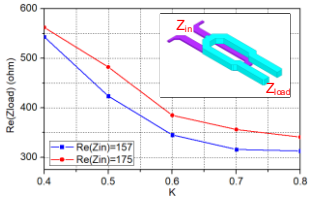

Fig. 5. The equivalent parallel resistance Zin and boosted Zload by tuning the coupling coefficient K of transformer.

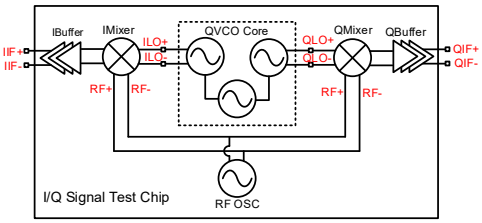

Fig. 6. Block diagram of I/Q signal test chip for phase and aptitude mismatch.

B. Passive Design and Integration

Another key aspect of high-frequency LC oscillator is the design and layout of transformers, as shown in Fig. 4. Different transformers play different roles. As discussed in section II, the top transformer (k2) is used to obtain maximum output power and DC-to-RF efficiency [9]. The transformers are drew as symmetric as possible to minimize common mode signal leakage to common source node to avoid disturbing the superharmonic signal injection operation. The bottom transformer is designed to push the oscillation frequency beyond 300 GHz and enlarge the injection signal level. As g_m is extremely small at high frequency, the priority is to satisfy the oscillation condition by boosting the parallel resistance presenting to the cross-coupled transistor pair without introducing extra inductance, which drops the operating frequency. Transformers at high frequencies are not easy to achieve large turn ratio due to the dimension constraint. The input impedance Z_{in} looking into the common-mode source nodes is obtained from simulation and listed in Fig. 5, and the equivalent parallel RC model is calculated as well. According to expressions (8) and (9), decreasing the coupling coefficient K is an effective way to boost R_p, as the curve shows in Fig. 5.

C. Phase and amplitude mismatch test scheme

Due to the lack of ultra-wideband oscilloscope to measure I/Q signal in G-band, the on-chip down-convertors are implemented to convert to IF for I/Q signal measurements [10]. Fig. 6 shows the block diagram with I/Q double-balanced mixers and buffers implemented on-chip. Besides, an additional

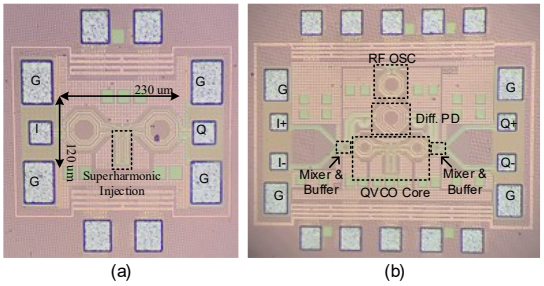

Fig. 7. Die micrographs of (a) the standalone QVCO and (b) I/Q test chips.

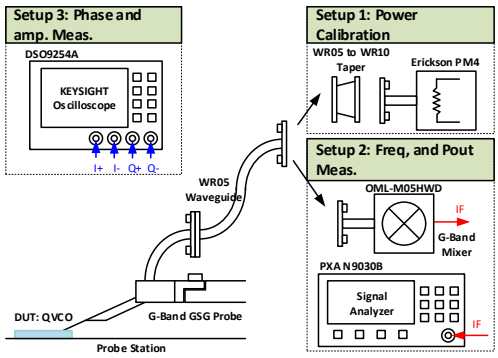

Fig. 8. Measurement setups for output power, frequency at G-band, and phase and amplitude error at down-converted frequency.

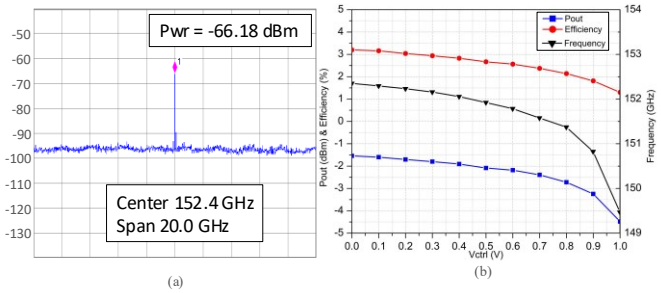

Fig.9. (a) Spectrum, (b) measured output power, DC-to-RF efficiency and oscillation frequency when tuning the bulk control voltage.

differential signal is generated as the LO to mix down the G-band I/Q signals. The buffers are realized with pseudo-differential neutralized source follower amplifiers, providing high input-output isolation, driving the off-chip 50 Ω for IF I/Q measurements.

IV. Experiment Results

Two chips, the standalone QVCO and I/Q signal test chip, have been fabricated in TSMC 28-nm bulk CMOS technology are shown in Fig. 7.

The output power, frequency and PN of the standalone QVCO were tested with Keysight N9030A spectrum analyzer through the external G-band harmonic mixer OML M05HWD and GGB probes, as shown in Fig. 8. The spectrum analyzer was calibrated and verified by an Erickson PM4 calorimeter. The standalone QVCO occupies an active area of only 0.028 mm^2. It consumes 21.9 mA from a 1V supply. Oscillation frequency covers from 149.3 to 152.4 GHz by tuning the body voltage from 0 to 1V. Fig. 9 shows the spectrum, measured output power and efficiency in the whole TR. It achieves the

Table 1. Comparison with state-of-the-art QVCO in mm-wave/sub-THz bands in silicon.

	Technology	Freq. (GHz)	Freq. TR (%)	DC Power (mW)	Pout (dBm)	Efficiency (%)	PN@1MHz (dBc/Hz)	Phase Error (◦)	Amp. Error (dB)	FOM_T[(a)] (dBc/Hz)	Area (mm^2)
[4]	28 nm CMOS	71.4-76.1/ 85.6-90.7	9.8	35.6	N/A	N/A	-114.2[(b)] -107[(b)]	1.5 3.5	1	-165.6	0.031
[7]	0.35um SiGe	55-76.5	32.7	1000	10.5	1.05	-97	13	N/A	-173.6	0.25
[11]	90nm CMOS	49-51.4	4.7	75.4	-10	0.13	-103.4	2.5	0.5	-172.2	1.47
[12]	65 nm CMOS	85-127	39.4	45	-15	0.07	-105[(b)]	2[(c)]	0.51[(c)]	-180.9	0.55
[13]	28 nm CMOS	37.5-45	18.2	8.4	-65	~0	-94.3	0.48[(d)]	N/A	-183	0.068
This work	28 nm CMOS	149.3-152.4	3.1	21.9	-1.54	3.2	-91.9	1.5	0.33	-168.3	0.028

(a) $FOM_T = \mathrm{PN} - 20\log\left(\frac{f_0}{\Delta f} \times \frac{TR}{10}\right) + 10\log\left(\frac{P_{DC}}{1mW}\right)$, (b) at 10 MHz offset, (c) simulated, (d) back-calculated

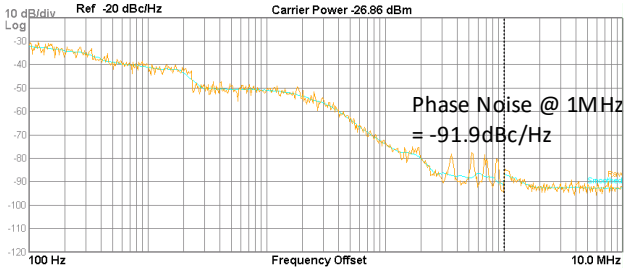

Fig. 10. Phase noise at the 152.4 GHz output.

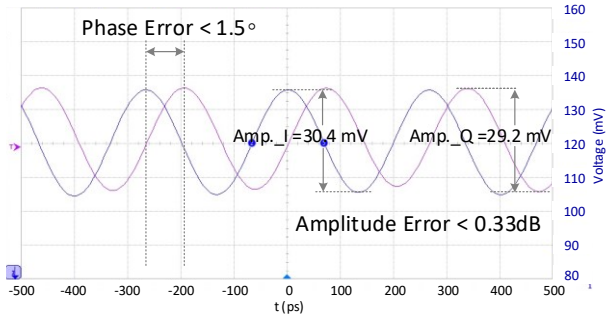

Fig. 11. Measured quadrature signals down-converted to 3.7GHz.

maximum power of -1.54 dBm with efficiency of 3.2% at 152.4 GHz. The measured PN is −91.9 dBc/Hz at 1 MHz offset for the 152.4 GHz output signal, as shown in Fig. 10. For the entire output frequency range, the PN is demonstrated is better than -90 dBc/Hz @ 1 MHz offset.

The IF I/Q signal from the test chip were measured by a Keysight oscilloscope DSO9254A. The downconverted IF outputs at 3.7GHz are shown in Fig. 11. Measurements repeated over the entire tuning range and demonstrated a phase error of less than 1.5◦ and amplitude mismatch less than 0.33 dB.

A comparison table with state of the art QVCOs in silicon in the mm-wave/sub-THz band is shown in Table 1. Benefited by the superharmonic injection technique and the design optimization for both active and passive devices, this work achieves the best I/Q phase accuracy, highest power efficiency and good PN for the entire tuning range.

V. Conclusion

A fully integrated G-band QVCO was successfully developed in a 28 nm CMOS process. Superharmonic injection structure and design optimization enable the proof-of-concept prototype to achieve accurate quadrature signals with phase error of less than 1.5◦ and amplitude error less than 0.33 dB for the entire frequency tuning range from 149.3 to 152.4 GHz. Optimizing the load impedance and transformers contribute to the measured power efficiency of 3.2%, which is the highest for QVCOs in mm-Wave/sub-THz bands. The measured PN is less than -90 dBc/Hz @ 1 MHz offset. The proposed QVCO will benefit the wide deployments of mm-wave/sub-THz systems, such as high-order modulation for ultra-high data rate communications, phase extraction of imaging and sensing.

VI. Acknowledgment

The authors would like to thank NSF for the financial support and TSMC for the chip fabrication.

References

[1] J. Gu, B. Yu, X. Ding, Y. Ye, X. Liu, and Z. Xu, “THz interconnect for inter-/intra-chip communication,” in *SPIE Defence + Commercial Sensing*, April, 2019.

[2] C. Jun Lee *et al.*, “A 120 GHz I/Q Transmitter Front-end in a 40 nm CMOS for Wireless Chip to Chip Communication,” in *IEEE RFIC Symp. Dig.*, Jule 2018, pp. 192-195.

[3] U. Decanis *et al.*, “A mm-Wave Quadrature VCO Based on Magnetically Coupled Resonators,” in *IEEE Int. Solid-State Circuits Conf. (ISSCC) Dig. Tech. Papers,* Feb. 2011, pp. 280-282.

[4] M. Vigilante *et al.*, “Analysis and Design of an E-Band Transformer-Coupled Low-Noise Quadrature VCO in 28-nm CMOS,” *IEEE Trans. Microw. Theory Tech.*, vol. 64, no. 4, pp. 1122-1132, April 2016.

[5] R. Han, S. Member, E. Afshari, and S. Member, “A CMOS High-Power Broadband 260-GHz Radiator Array for Spectroscopy,” *IEEE J. Solid-State Circuits*, vol. 48, no. 12, pp. 3090-3104, Dec. 2013.

[6] T. M. Hancock and G. M. Rebeiz, “A novel superharmonic coupling topology for quadrature oscillator design at 6 GHz,” *2004 IEEE RFIC Symp. Dig.*, June 2004, pp. 285-288.

[7] I. Nasr, M. Dudek, R. Weigel, and D. Kissinger, “A 33% Tuning Range High Output Power V-Band Superharmonic Coupled Quadrature VCO in SiGe Technology,” in *IEEE RFIC Symp. Dig.*, June 2012, pp. 301-304.

[8] B. Razavi, “A Study of Injection Locking and Pulling in Oscillators,” *IEEE J. Solid-State Circuits*, vol. 39, no. 9, pp. 1415-1424, Sept. 2004.

[9] Y. Ye, B. Yu, X. Ding, X. Liu and Q. J. Gu, "High energy-efficiency high bandwidth-density sub-THz interconnect for the “Last-Centimeter” chip-to-chip communications," in *IEEE MTT-S Int. Microw. Symp. Dig.,* June 2017, pp. 805-808.

[10] S. Hao *et al.*, “An Active Circulator-Based Delay Line,” *IEEE Microw. Wireless Compon. Lett.*, vol. 29, no. 7, pp. 492-494, July 2019.

[11] H.-Y. Chang *et al.*, “Design and Analysis of CMOS Low-Phase-Noise Low Quadrature Error V-Band Subharmonically Injection-Locked Quadrature FLL,” *IEEE Trans. Microw. Theory Tech.*, vol. 66, no. 6, pp. 2851-2866, June 2018.

[12] J. Zhang *et al.*, “85-to-127 GHz CMOS Signal Generation Using a Quadrature VCO With Passive Coupling and Broadband Harmonic Combining for Rotational Spectroscopy,” *IEEE J. Solid-State Circuits*, vol. 50, no. 6, pp. 1361-1371, June 2015.

[13] L. Zhang, N. Kuo and A. M. Niknejad, “A 37.5–45 GHz Superharmonic-Coupled QVCO With Tunable Phase Accuracy in 28 nm CMOS,” *IEEE J. Solid-State Circuits*, vol. 54, no. 10, pp. 2754-2764, Oct. 2019.